Cell Stem Cell
Article

Functional Genomics Reveals a BMP-Driven Mesenchymal-to-Epithelial Transition in the Initiation of Somatic Cell Reprogramming

Payman Samavarchi-Tehrani,[1,3,4] Azadeh Golipour,[1,3,4] Laurent David,[1,4] Hoon-ki Sung,[2] Tobias A. Beyer,[1] Alessandro Datti,[1] Knut Woltjen,[2,5,*] Andras Nagy,[2,3,*] and Jeffrey L. Wrana[1,3,*]
[1]Center for Systems Biology
[2]Center for Stem Cells and Tissue Engineering
Samuel Lunenfeld Research Institute, Mount Sinai Hospital, Toronto, Ontario M5G 1X5, Canada
[3]Department of Molecular Genetics, University of Toronto, Ontario M5S 1A8, Canada
[4]These authors contributed equally to this work
[5]Present address: Center for iPS Cell Research and Application (CiRA), Institute for Integrated Cell-Material Sciences (iCeMS), Kyoto University, Kyoto 606-8507, Japan
*Correspondence: woltjen@cira.kyoto-u.ac.jp (K.W.), nagy@lunenfeld.ca (A.N.), wrana@lunenfeld.ca (J.L.W.)
DOI 10.1016/j.stem.2010.04.015

SUMMARY

Somatic cells can be reprogrammed to induced pluripotent stem cells (iPSCs) by expression of defined embryonic factors. However, little is known of the molecular mechanisms underlying the reprogramming process. Here we explore somatic cell reprogramming by exploiting a secondary mouse embryonic fibroblast model that forms iPSCs with high efficiency upon inducible expression of Oct4, Klf4, c-Myc, and Sox2. Temporal analysis of gene expression revealed that reprogramming is a multistep process that is characterized by initiation, maturation, and stabilization phases. Functional analysis by systematic RNAi screening further uncovered a key role for BMP signaling and the induction of mesenchymal-to-epithelial transition (MET) during the initiation phase. We show that this is linked to BMP-dependent induction of miR-205 and the miR-200 family of microRNAs that are key regulators of MET. These studies thus define a multistep mechanism that incorporates a BMP-miRNA-MET axis during somatic cell reprogramming.

INTRODUCTION

The capacity of differentiated cells to reacquire a totipotent state was first revealed when the nuclei of differentiated cells were reprogrammed in enucleated oocytes to generate frogs (Gurdon, 1964). Furthermore, ectopic expression of just four transcription factors, Oct4, Klf4, c-Myc, and Sox2 (OKMS), is sufficient to reprogram somatic cells to induced pluripotent stem cells (iPSCs) (Takahashi and Yamanaka, 2006). Fully reprogrammed iPSCs have a similar developmental potential as embryonic stem cells (ESCs) and can contribute extensively to the three germ layers and the germline (Zhao and Daley, 2008). At the molecular level, reprogramming results in large changes in gene expression that remodel the somatic cell properties to a state similar to embryonic stem cells (Maherali et al., 2007; Mikkelsen et al., 2008; Sridharan et al., 2009) that include early activation of the pluripotency markers alkaline phosphatase (AP) and SSEA1 (Brambrink et al., 2008) followed by embryonic stem cell factors such as Oct4, Sox2, and Klf4 themselves, as well as Nanog and Sall4 (Maherali et al., 2007; Okita et al., 2007; Wernig et al., 2007; Xu et al., 2009). Nanog is a component of the stem cell regulatory network that is critical for acquiring the pluripotent state during somatic cell reprogramming (Silva et al., 2009). Furthermore, failure to suppress differentiation-associated genes or block differentiation signals leads to incomplete reprogramming (Mikkelsen et al., 2008).

Although a considerable amount is known about the transcriptional networks that regulate ESCs, relatively little is known of the signaling pathways that integrate intrinsic and extrinsic cues to maintain the pluripotent state and control reprogramming. TGF-β-related factors that include the bone morphogenetic proteins (BMPs) are an important family of morphogens that regulate cell fate decisions in stem cells (Varga and Wrana, 2005). In the BMP pathway, ligand binding to the heterotetrameric complexes of type II and type I receptors leads to phosphorylation of receptor-regulated R-Smads 1, 5, and 8 that in turn bind to Smad4 and accumulate in the nucleus to regulate transcription (Attisano and Wrana, 2002). In mouse ES cells (mESCs), BMP signaling together with leukemia inhibiting factor (LIF) signaling is important for maintaining the pluripotent state (Ying et al., 2003), whereas TGF-β/Activin signaling is critical in human ESCs and mouse stem cells that are derived from the epiblast (EpiSC) (Vallier et al., 2009). Interestingly, TGF-β receptor-specific small molecule antagonists were recently shown to promote reprogramming by promoting Sox2- and Myc-dependent functions (Ichida et al., 2009; Maherali and Hochedlinger, 2009). TGF-β and BMPs may thus play important regulative roles in controlling distinct stem cell states and reprogramming.

Understanding the process of reprogramming and in particular the signaling networks that control progression to a stable pluripotent state has been hampered in part by the low frequency of the event. Here we employed mouse iPSCs generated with

a *piggyBac* transposon system that expresses OKMS in a doxycycline (Dox)-inducible manner (Woltjen et al., 2009). Secondary mouse embryonic fibroblasts (2° MEFs) from *piggyBac* iPSC-derived chimeras reprogram efficiently, thus allowing us to apply temporal gene expression profiling coupled to a functional siRNA screen to dissect mechanisms underlying the early stages of reprogramming. This integrative approach reveals three phases of reprogramming that we term initiation, maturation, and stabilization and uncovers an early mesenchymal-to-epithelial transition (MET) that marks initiation. Furthermore, we show that BMP signaling synergizes with OKMS to induce a microRNA (miRNA, miR-) expression signature that is associated with MET and promotes progression through the initiation phase. These studies unveil broad temporal alterations in gene expression during reprogramming and define a critical initiation phase that is regulated by a BMP-miRNA-MET signaling axis.

RESULTS

Gene Expression Profiling Reveals Three Phases of Reprogramming

Reprogramming of primary murine somatic cells by ectopic expression of OKMS occurs at low frequency, making the molecular characterization of reprogramming difficult. However, reprogramming occurs in secondary systems with much higher efficiencies (Maherali et al., 2008; Wernig et al., 2008; Woltjen et al., 2009). Recently, we established a reprogramming system with Dox-regulated OKMS transgenes delivered via *piggyBac* transposition (Woltjen et al., 2009). Chimeric mice from two primary iPSC lines (6C and 1B) were used to isolate chimeric 2° MEF lines (2°-6C and 2°-1B MEFs) in which the GFP$^+$, iPSC-derived 2° MEFs reprogrammed with high efficiency upon Dox induction (see schematic, Figure 1A). We confirmed the pluripotency of iPSCs derived from the 2°-6C MEFs via embryoid body assays, teratomas, and contribution to diploid chimeric embryos (Figure S1 available online). iPSCs derived from 2°-1B MEFs also contributed extensively to adult chimeric mice (Figure S1E). Thus, secondary iPSCs generated from the *piggyBac* system are pluripotent, like their primary counterparts.

Because our secondary iPSC system reprograms with high efficiency (Woltjen et al., 2009), we sought to characterize changes in the transcriptome during reprogramming of 2°-6C cell line by microarray analysis at 2, 5, 8, 11, 16, and 21 days after OKMS induction (Table S2). Comparison of the starting MEF population and their iPSC progeny revealed 4,252 genes, out of the 13,389 genes detected, changed expression more than 2-fold with 3,520 genes upregulated and only 732 downregulated. Of these, 61% were the same as those identified in a previous analysis of MEF reprogramming (Sridharan et al., 2009), indicating good concordance between the two studies. We next analyzed the Pearson correlation coefficient (PCC) of the transcriptional profile, which showed increasing similarity to the primary iPSC profile through the course of reprogramming (Figure 1B), and unsupervised clustering revealed segregation into temporally distinct early, middle, and late phases (Figure 1B). To further resolve these temporal changes, we clustered genes based on when expression changes occurred (Figure 1C). This showed that a large number of genes changed expression early in the time course of reprogramming (clusters I and II), as well as distinct subsets of genes that were altered at later time points. Embryonic stem cell-associated genes clustered into either the middle or late phases (Table S1) and their patterns of expression were validated by qPCR (Figure S2A). *Nanog*, an exemplar of the middle cluster, initiated expression after day 5 and then rapidly climbed to a high level that was sustained throughout the reprogramming time course, peaking in 2°-6C iPSCs at levels comparable to primary 6C iPSCs (Figure S2A). *Sall4* and *Esrrb* shared *Nanog*'s expression pattern. Similarly, *Rex1, Tcl1, Nodal*, and *Cripto* were expressed at high level in the middle phase although their expression initiated slightly later. In contrast, the late-phase cluster was characterized by induction of *Dnmt3l, Lin28*, *Utf1*, and slightly later by *Pecam*, *Stella*, and *Dppa4* (Furusawa et al., 2006; Müller et al., 2008). Altogether, these studies reveal three phases during OKMS-induced MEF reprogramming that we refer to as initiation, maturation, and stabilization (Figure S2B). Interestingly, no embryonic stem cell factors were expressed in the initiation phase, while the maturation phase, as marked by the beginning of *Nanog*, *Sall4*, *Esrrb*, *Rex1, Tcl1, Cripto*, and *Nodal* expression, occurred at approximately day 8, and the stabilization phase, marked by *Dnmt3l, Lin28, Utf1, Pecam*, *Stella*, and *Dppa4*, started at around day 21.

The Initiation Phase Is Elastic

Nanog drives the broad changes in the transcriptional program that are associated with the acquisition of pluripotency (Mitsui et al., 2003; Sridharan et al., 2009) and can push pre-iPSCs to the pluripotent state (Silva et al., 2009). *Nanog* is not expressed until after day 5 in our reprogramming system, suggesting that the initiation phase might not be self-sustaining. Indeed, SSEA1 induction and morphological changes induced by OKMS are rapidly lost when OKMS expression is suppressed early in reprogramming (Brambrink et al., 2008; Woltjen et al., 2009). We therefore explored whether the initiation phase was elastic, thus allowing cells to reattain their parental gene expression profile upon OKMS removal. For this, we induced OKMS for 5 days, followed by 5 days of OKMS withdrawal (Figure 1D). Comparative analysis by PCC (Figure 1D) revealed that 2°-1B and 2°-6C parental MEFs were most similar to each other (PCC = 0.97) and to primary MEFs (PCC = 0.95 and 0.94, respectively). OKMS induction led to a divergence of the gene expression profile of 2°-1B cells (PCC = 0.86), with 3421 genes altered greater than 2-fold. Remarkably, after OKMS withdrawal, 88% of these genes reverted back to expression levels observed in the starting MEF population (Figure S2C; Figure 1D; PCC = 0.97). These results indicate that the initiation phase is not self-sustaining and is elastic, thus allowing rapid reversion to a differentiated state once OKMS expression is removed.

MET Is a Hallmark of the Initiation Phase

The molecular events in the early phases of reprogramming are poorly understood. We therefore focused on the initiation phase, which is induced over the first 5 days of reprogramming, and noted induction of a large number of epithelial-associated genes. These genes include the epithelial junctional protein E-cadherin (*Cdh1*), as well as *Cldns -3*, *-4*, *-7*, *-11*, Occludin (*Ocln*), Epithelial cell adhesion molecule (*Epcam*), and Crumbs homolog 3 (*Crb3*), all of which are components of epithelial junctions (Figure 1C). These results, which were validated by qPCR (Figure 2A), led

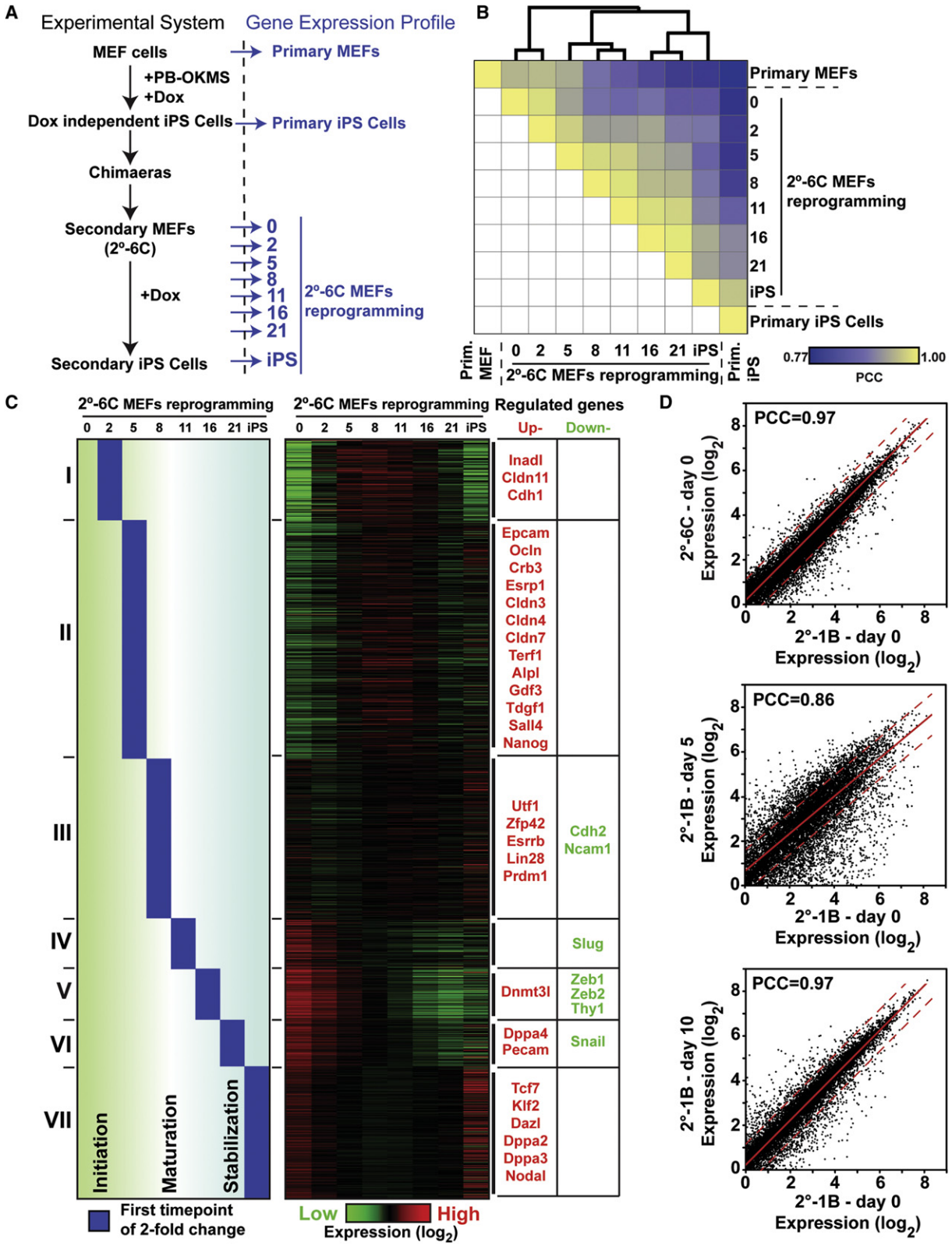

Figure 1. Expression Profiling Reveals Three Phases of Reprogramming

(A) Schematic of experimental system and time points of microarray analysis.

(B) Hierarchical clustering of expressed genes throughout reprogramming of 2°-6C MEFs. Microarray analysis from each of the indicated time points were compared against each other via Pearson correlation coefficient (PCC) and are plotted as a heat map matrix. Samples were also clustered by unsupervised

us to investigate the expression of the mesenchymal regulators: Zn finger transcription factors Snail, Slug, Zeb1, and Zeb2. These factors maintain the mesenchymal phenotype by directly repressing epithelial gene expression (Thiery et al., 2009). Consistent with the gain of epithelial-like markers, these transcription factors were repressed in reprogramming 2°-6C cultures and paralleled the loss of the fibroblast markers Cdh2 and Thy1 (Figure 2A). These findings suggest that initiation of MEF reprogramming involves a mesenchymal-to-epithelial transition (MET). To confirm this, we initiated reprogramming for 5 days and stained early reprogramming colonies with phalloidin, which stains F-actin, together with β-catenin and Cdh1, both of which mark adherence junctions (Figure 2B). In parental MEFs, F-actin was organized into stress fibers characteristic of fibroblasts, Cdh1 expression was undetectable, and β-catenin was diffusely cytosolic and localized to puncta. In contrast, after OKMS induction, colonies with cortical F-actin and both β-catenin and Cdh1 in cell junctional regions were readily apparent, similar to fully reprogrammed 2°-6C iPSC colonies (Figure 2B, arrows). At 5 days, all colonies were positive for AP and SSEA1, both markers of early reprogramming (Figures S3A and S3B). To further confirm MET in reprogramming cells, we FACS-sorted SSEA1-positive (SSEA1$^+$) cells 5, 8, and 11 days after OKMS induction and observed that *Cdh1*, *Epcam*, *Crb3*, and *Ocln* were all strongly induced in SSEA1$^+$ cells (Figure 2C). We confirmed that these cells also express *Nanog*, *Sall4*, and *Oct4*, but not until day 8 (Figure S3C). Conversely, *Snail*, *Slug*, *ZEB1*, and *ZEB2* were all strongly repressed. The initiation phase of fibroblast reprogramming is thus characterized by a coordinated MET that precedes the upregulation of ESC markers.

A Functional RNAi Screen for Regulators of Reprogramming Initiation

To understand how the transcriptional program induced by OKMS drives the initiation phase of reprogramming, we next devised a systematic genetic RNAi screen with 2°-6C cells. To optimize assay parameters, we used Oct4 siRNA as a positive control and dharmacon control siRNA and Nanog siRNA, which is not induced until after initiation, as negative controls. After transfection, cells were cultured in the presence of Dox for 5 days, after which colonies were stained for AP, an early marker of pluripotency (Brambrink et al., 2008; Okita et al., 2007; Takahashi and Yamanaka, 2006), and DAPI to identify nuclei (Figure 3A). Knockdown of Oct4, which is expressed from the integrated *piggyBac* transposon, inhibited colony formation (Figure S4A). In contrast, Nanog siRNA had no effect, consistent with its lack of expression at this early phase. We then developed an automated image analysis strategy to identify colonies based on the distribution of nuclei and AP counterstaining (Figure 3A) and optimized parameters via mock, control, Nanog, and Oct4 transfectants (Figure S4B). Because of the limited proliferative potential of primary cells, we were not able to conduct a genome-wide screen, so we generated a custom siRNA library that targets all signaling genes, transcription factors, and chromatin regulators (4010 genes; Table S3). Each siRNA was assessed in replicate, the results were averaged, and those with less than 15% covariance plotted (Figure 3B). Only 413 siRNA showed covariance greater than 15%, indicating excellent concordance between replicates and a robust screen. Analysis of screen data revealed that knockdown of four Yamanaka factors, Oct4, Klf4, c-Myc, and Sox2, that were present in the library suppressed reprogramming to varying extents (Figure 3B). Of note, p53 knockdown enhanced formation of colonies (Figure S4C), consistent with recent studies showing that p53 suppresses reprogramming (Zhao and Xu, 2010).

To gain mechanistic insight into key events required for progression through the initiation phase, we explored the siRNAs that suppressed or abolished colony formation. Interestingly, analysis of genes associated with MET revealed that siRNAs targeting Cdh1 and the polarity complex components, Par3 and Crb3, all strongly suppressed the appearance of AP-positive reprogramming colonies (Figure 3C). These findings suggest that MET is a functionally important early event during reprogramming. We also wanted to gain insight into signaling pathways that might regulate initiation and found that knockdown of Smad1, which is a key transcriptional mediator of signaling by BMPs, suppressed formation of AP-positive colonies (Figure 3D). Furthermore, knockdown of the Smad1 partner, Smad4, also inhibited reprogramming, as did knockdown of the BMP type II receptor, BMPRII, and the BMP type I receptor, ALK3 (Figure 3D). We confirmed that the siRNA pools to both the epithelial and BMP pathway components efficiently knocked down their targets and tested the individual siRNAs that comprise the pool, most of which efficiently reduced expression of their target and inhibited reprogramming (Figure S5). These results suggest that efficient progression through the initiation phase of reprogramming is dependent on MET and BMP signal transduction.

BMP Signaling Promotes Reprogramming

Our functional genomics screen implicated the BMP pathway as a key regulator of reprogramming initiation, though no exogenous BMP is added to the media. However, BMP derived from serum, the cocultured MEFs, or the reprogramming cells

hierarchical clustering with complete linkage PCC and the dendrogram of similarity relationship is shown above the heat map. Note the three predominant groupings.

(C) Clustering of gene expression profiles based on kinetics of change. Gene expression data are shown for all genes that changed greater than 2-fold during the reprogramming time course, as indicated. Data were clustered according to the first time point of ≥2-fold change (blue, left), and the corresponding median-centered $\log_2$ expression profile is represented via a heat map (right) according to the scale. Sample gene names from each cluster that are up- or downregulated (red or green, respectively), in 2°-6C iPS cells relative to 2°-6C MEFs, are shown. The color gradient shows the three phases: initiation, maturation, and stabilization.

(D) The initiation phase of reprogramming is elastic. 2°-1B MEFs were treated for 5 days with Dox followed by 5 days of Dox withdrawal and gene expression analyzed by microarray analysis. Data for the indicated samples were plotted as paired scatter plots. The line of best fit is shown in solid red, with 2-fold differential expression delineated by the dashed lines. PCC values are indicated (top left corner of each graph). Note that the scattering of gene expression upon 5 days of Dox treatment of 2°-1B cells returns to the parental profile after removal of Dox.

See also Figures S1 and S2.

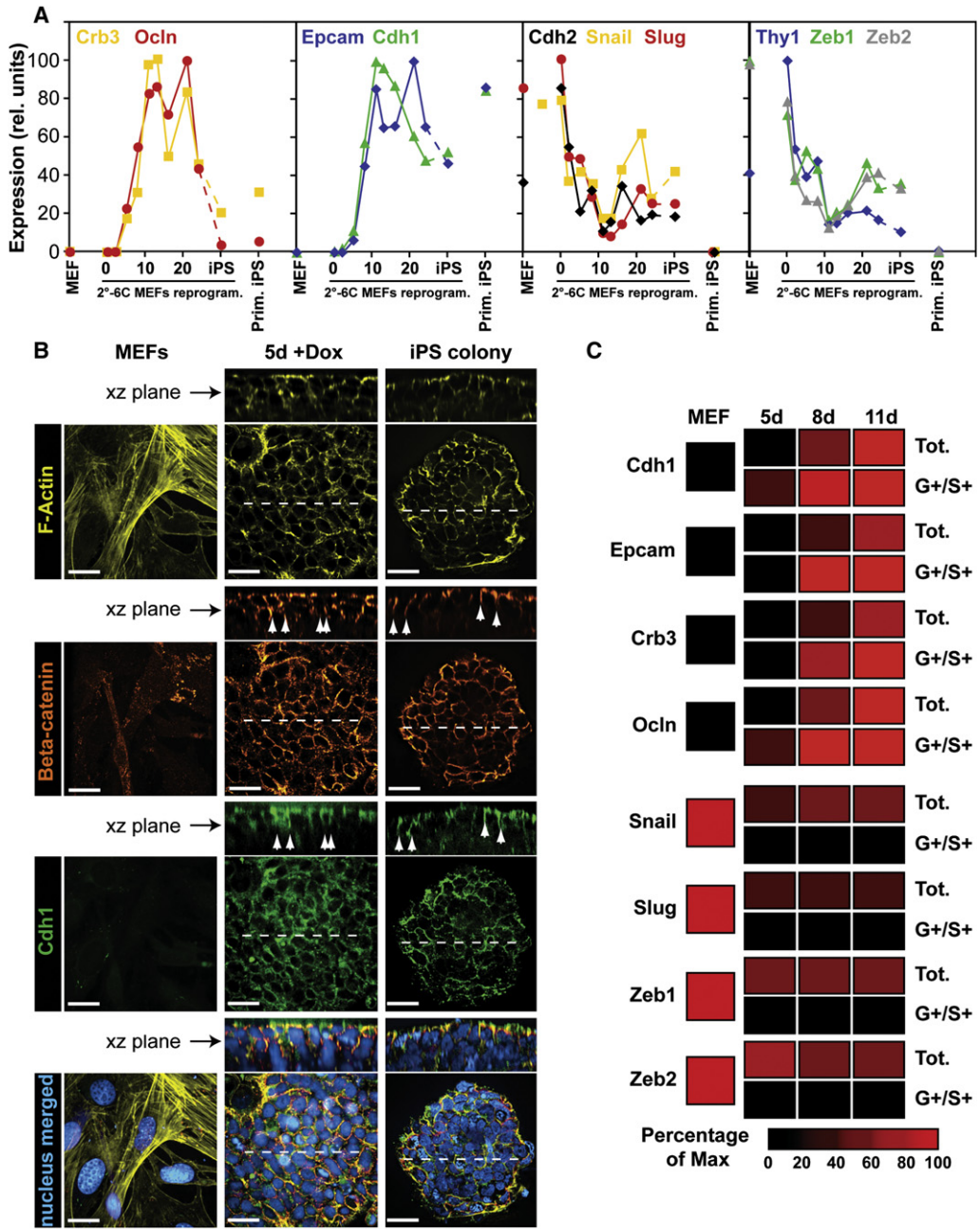

Figure 2. MET Occurs during the Initiation Phase

(A) Expression pattern for MET signature genes. Expression profiles for the indicated epithelial (Crb3, Ocln, Epcam, and Cdh1) and mesenchymal (Cdh2, Snail, Slug, Thy1, Zeb1, Zeb2) genes were determined by RT-qPCR analysis of the 2°-6C reprogramming time course samples and are plotted as indicated. Data from primary MEFs and 2°-6C primary iPSCs serve as reference points (nonconnected points).

(B) Epithelial-like characteristics in reprogramming cells and iPSC colonies. 2°-6C MEFs untreated (MEFs) or treated with Dox for 5 days, as well as fully reprogrammed 2°-6C iPSCs, were fixed and stained for F-actin (yellow), β-catenin (orange), Cdh1 (green), and nuclei (blue) and imaged by confocal microscopy. Individual stains and a merged image of an XY plane and the indicated Z-stack are shown. White arrows point to cell junctions and white dashed lines represent the z plane shown above each of the panels. Scale bars represent 25 μm.

(C) SSEA1$^+$ reprogramming cells undergo MET. 2°-6C MEFs treated for 5, 8, or 11 days with Dox were FACS sorted to isolate the GFP$^+$/SSEA1$^+$ population (G$^+$/S$^+$) and gene expression analyzed by RT-qPCR. qPCR results for the indicated genes are represented as a heat map from black (minimum levels) to red (maximum levels) and are compared against the total (Tot.) unsorted population analyzed in parallel. Note the enrichment for epithelial markers and downregulation of mesenchymal markers in the sorted versus total populations.

See also Figure S3.

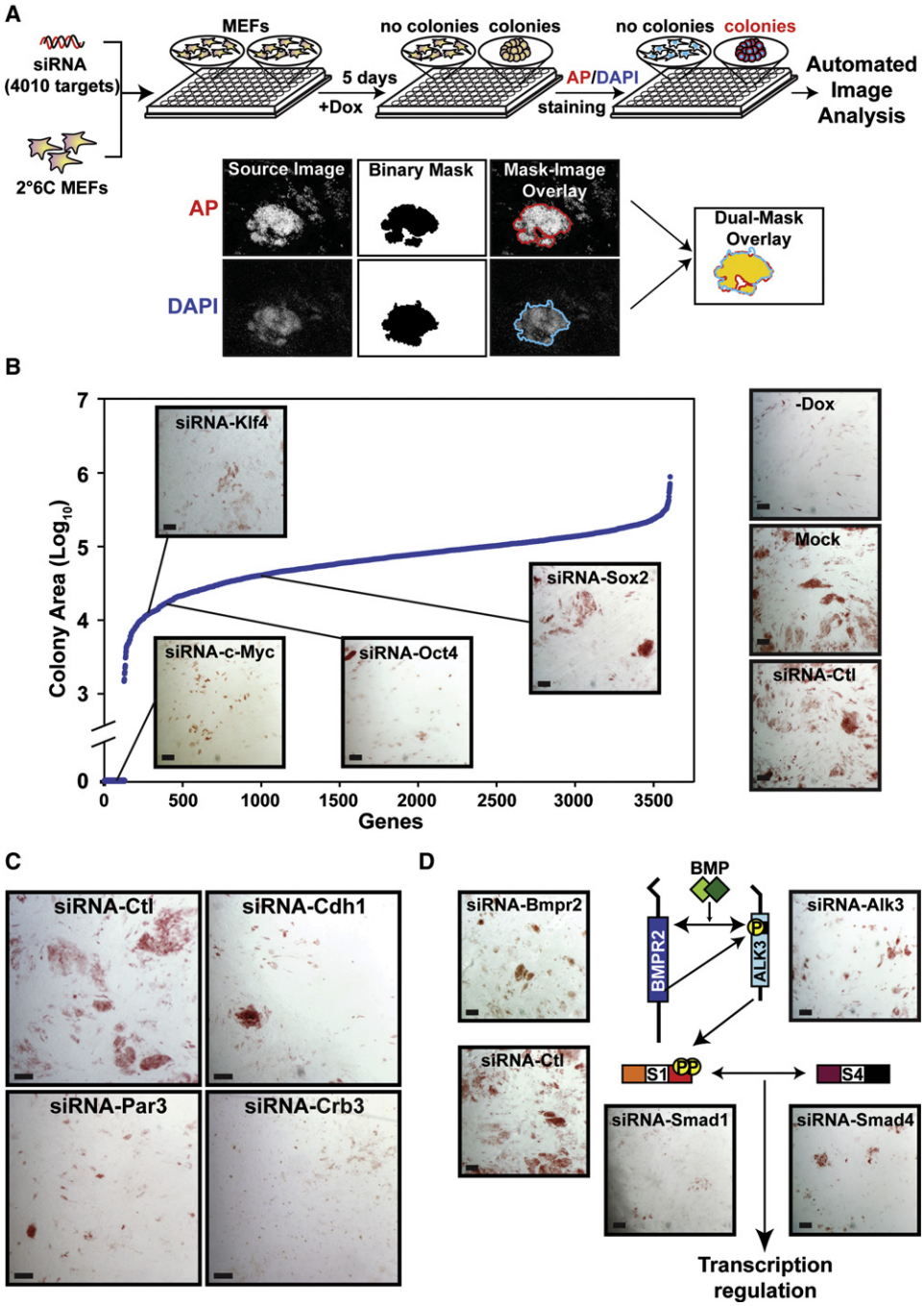

Figure 3. A Phenotypic siRNA Screen for Regulators of Reprogramming Initiation

(A) Schematic of functional siRNA screen to identify regulators of the initiation phase. 2°-6C MEFs were transfected in 96-well plates, with each individual well receiving a single siRNA designed to target one of 4010 distinct genes. OKMS was induced and cells were fixed and stained for AP and DAPI after 5 days. Images were acquired with an InCell-1000 high-content microscope and the overlap of the dual AP/DAPI colony area mask was quantified as shown.

(B) Results of the siRNA screen. The colony area of replicate siRNA transfections were averaged and those with less than 15% coefficient of variance were plotted as a rank-order plot of $\log_{10}$ transformed values. Representative AP-stained images of the Oct4, Klf4, c-Myc, and Sox2 siRNAs are shown as insets. For comparison, representative AP-stained images of non-Dox-treated and Dox-treated mock and control siRNA transfected 2°-6C cells are shown on the right.

(C and D) Components of epithelial polarity complexes and the BMP signaling pathway inhibit initiation. Representative AP-stained images from the siRNA screen targeting components of epithelial polarity (Cdh1, Par3, Crb3) are shown in (C). Schematic of the BMP-Smad signaling pathway showing ligand (green), type II receptor (dark blue), type I receptor (cyan), Smad1, and Smad4 (orange and maroon, respectively). Representative AP-stained images from the siRNA screen targeting each of the indicated components and a control (Ctl) are shown in (D).

Scale bars represent 200 μm. See also Figures S4 and S5.

themselves might activate the pathway. To examine this, we analyzed the receptor-activated form of Smad1 with a phospho-specific antibody, which revealed strong Smad1 activation in reprogramming MEFs that was blocked by the BMP receptor antagonist, dorsomorphin (Figure 4A). Dorsomorphin has poor specificity, so we also used the soluble BMP ligand antagonists Noggin (Herrera and Inman, 2009) and the extracellular domain of ALK1 (A1ECD) (David et al., 2008). Each alone decreased Smad1 activation, while together they strongly suppressed the pathway. Thus, intrinsic BMP signaling occurs during the initiation phase of reprogramming.

We next examined whether supplementing BMP or suppressing intrinsic BMP signaling with Noggin/A1ECD-modulated reprogramming. In the absence of OKMS expression, BMP2, BMP7, or BMP9 failed to induce AP in 2°-6C MEFs, whereas they enhanced AP-positive colonies in the presence of Dox-induced OKMS (Figure S6A). Similarly, FACS analysis revealed 41% of OKMS-expressing cells were SSEA1$^+$ by day 5, while BMP7 strongly enhanced the proportion to 68% of the population (Figures 4B and 4C). In stark contrast, only 26% of Noggin/A1ECD-treated cells were SSEA1$^+$ and almost no SSEA1$^+$ colonies were observed (Figures 4B and 4C). Of note, SSEA1 was not induced by BMP7 in the absence of OKMS (Figure S6B). Finally, we examined primary MEFs transfected with OKMS-expressing *piggyBac* transposons and observed that 2 nM BMP7 stimulated formation of reprogramming colonies by 3-fold (Figure 4D). We also confirmed that reprogrammed primary iPSCs, which were treated with BMP7 during the initiation phase, successfully produced adult chimeric mice (Figure 4E).

Our results show that BMP signaling promotes the early stage of reprogramming. This was not due to regulation of proliferation as assessed by phospho-histone H3 (Figure S6Ci) and CyQuant staining (Figure S6Cii). However, *Sall4*, *Nanog*, and endogenous *Oct4* all showed enhanced expression upon BMP stimulation that was reduced by BMP antagonism (Figure 5A). Importantly, these genes were not induced by BMP in the absence of OKMS induction. BMP thus synergizes with OKMS to stimulate the onset of *Nanog* and *Sall4* expression. Nanog is required for (Brambrink et al., 2008) and Sall4 promotes (Tsubooka et al., 2009) acquisition of the reprogrammed phenotype and cells that fail to reprogram display low or absent Nanog (Silva et al., 2009; Sridharan et al., 2009). We therefore tested whether BMP promotes transition to a stably reprogrammed phenotype by evaluating the timing and number of Dox-independent colonies formed after OKMS induction. For this, we induced OKMS for either 6 or 9 days in the presence or absence of BMP7 and then removed Dox until day 15 when we assessed colony formation (Figure 5B). In controls, Dox-independent colonies were observed only in day 9 samples, consistent with our gene expression analysis that mapped the initiation-maturation phase transition to between days 6 and 8. In contrast, BMP7-stimulated formation of Dox-independent colonies by day 6 and further increased the colony count by day 9 (Figure 5B). Single-cell assays also showed that brief BMP7 treatment during the early phase enhanced the formation of AP-positive, Dox-independent colonies at day 18 (Figure 5C). BMP thus stimulates reprogramming by accelerating progression to the maturation phase.

BMP Induces MET and Its Regulators, miR-205 and the miR-200 Family of miRNAs

We identified both MET and BMP signaling as key components of the initiation phase of reprogramming, leading us to consider whether BMP signaling might synergize with OKMS to promote MET during the initiation phase. In control and BMP7-stimulated reprogramming colonies, Cdh1 expression was strong (Figure 6A), while colonies that formed in the absence of BMP signaling had little or no Cdh1 protein (Figure 6A, arrows) or *Cdh1* mRNA (Figure 6B). *Epcam* and *Ocln* expression were also strongly dependent on BMP signaling. Moreover, BMP-dependent expression of these epithelial genes required OKMS as indicated by the fact that none were induced by BMP7 in the absence of Dox (Figure 6B). Recent studies have highlighted a key role for the microRNAs, miR-205 and the miR-200 family, in regulating MET via direct downregulation of Zeb1 and Zeb2 (Bracken et al., 2008; Gregory et al., 2008; Korpal et al., 2008). Therefore, we examined the expression of miR-205 and the miR-200 family members, miR-141, miR-200a, miR-200b, miR-200c, and miR-429 (Figure 6C), all of which were induced by OKMS during initiation phase and were strongly suppressed by inhibition of BMP signaling. Furthermore, exogenous BMP7 enhanced expression of miR-200a, -200b, and -205, but only in the presence of OKMS, whereas miR-141, -200c, and -429 displayed little further induction, suggesting that the level of intrinsic BMP signaling is sufficient to drive full expression of the latter group. Altogether, these results demonstrate that BMPs synergize with OKMS to induce a broad program of miRNA expression that is associated with MET.

Because of the large number of MET-associated miRNAs induced during reprogramming, we were not able to employ miRNA antagonists to interfere with their function. Therefore, we tested whether two miR-200 family mimics (Mim-200b and Mim-200c) might stimulate MET and promote MEF reprogramming. Transfection of MEFs with either Mim-200b or Mim-200c alone or together strongly induced *Cdh1*, *Epcam*, and *Ocln* expression and suppressed *Zeb1* and *Zeb2* expression, as previously shown (Korpal et al., 2008), as well as *Snail* and *Slug* (Figure 7A). Time-course analysis of reprogramming MEFs further revealed that Mim-200b and Mim-200c enhanced induction of *Cdh1* and *Epcam* by OKMS (Figure 7B). Next we examined early reprogramming events by analyzing SSEA1 induction via FACS. In mock and Mim-control transfected cells, 45% of the population was SSEA1$^+$, whereas in Mim-200b- or Mim-200c-transfected populations, 64% of the cells were SSEA1$^+$ (Figure 7C). We also examined *Nanog* and *Sall4*, both of which showed strongly enhanced expression and earlier induction in the presence of Mim-200b and Mim-200c (Figure 7D). As in the case of BMP stimulation, the miR-200 mimics did not induce *Nanog* or *Sall4* in the absence of OKMS (data not shown). iPSCs derived from mimic-treated reprogramming MEFs were also chimera competent (Figures S7A and S7B). Induction of miR-205 and miR-200 family expression thus stimulates MET and synergizes with OKMS to accelerate progression through the initiation phase of reprogramming.

Finally, we asked whether inducing MET via miR-200 family mimics rescues the inhibition of reprogramming by BMP antagonists. For this we induced OKMS for 5 days and quantified SSEA1$^+$ cells in the population (Figure 7E). As previously, BMP antagonists suppressed reprogramming efficiency from 33% to 22% of the population. In contrast, MEFs transfected with

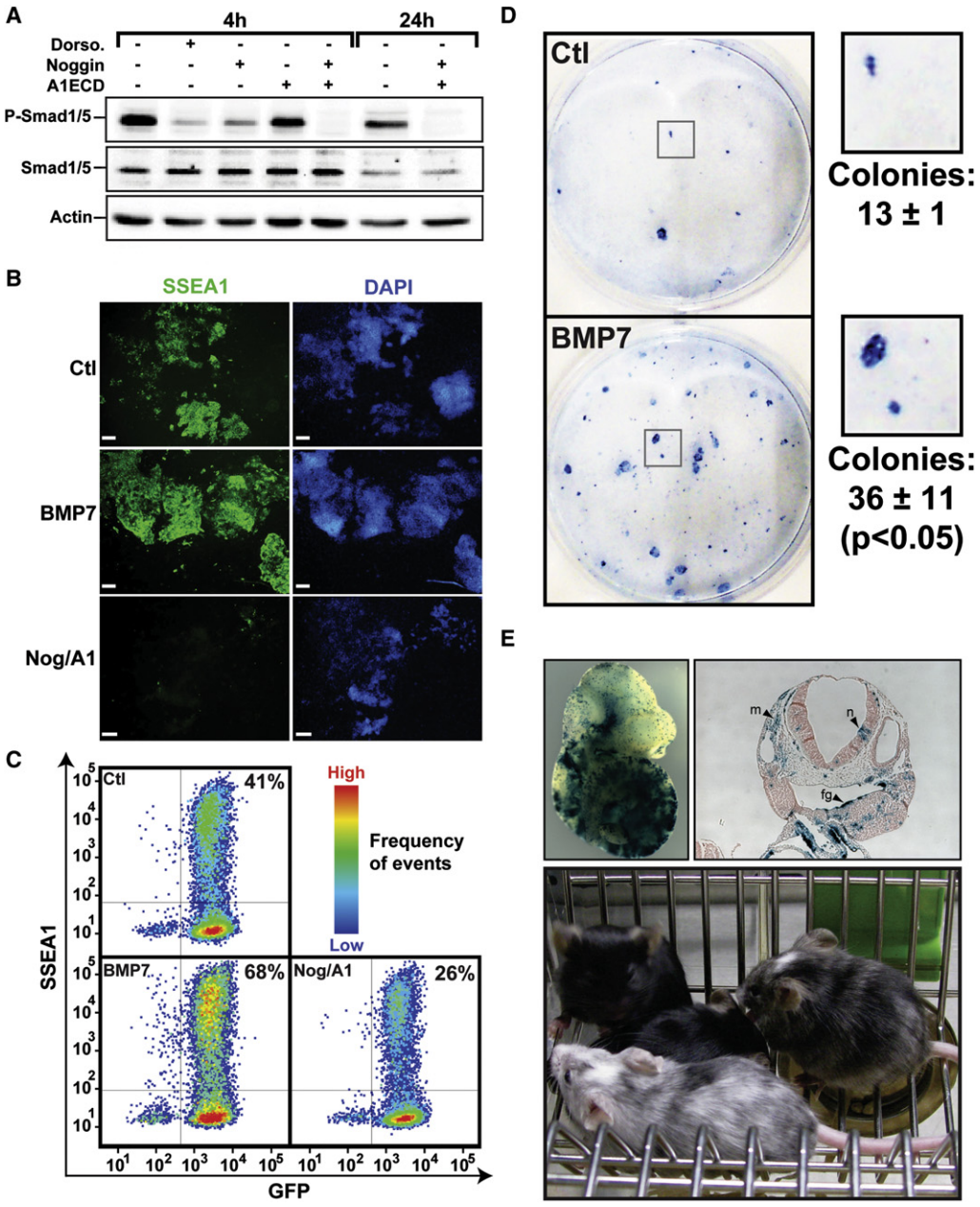

Figure 4. BMP Signaling Promotes Reprogramming

(A) The BMP-Smad1 pathway is active during reprogramming. 2°-6C MEFs were seeded overnight in mESC media, then treated as indicated, with dorsomorphin (5 μM), Noggin (2 nM), ALK1 extracellular domain (A1ECD; 1 nM) for 4 hr. Cell lysates were immunoblotted with antibodies to Phospho-Smad1/5, Smad1/5, and Actin.

(B and C) BMP signaling stimulates formation of SSEA1$^+$ colonies. 2°-6C MEFs were treated for 5 days with Dox in presence or absence of BMP7 (2 nM) or Noggin and A1ECD (Nog/A1), fixed in PFA, and analyzed by immunofluorescence after SSEA1/DAPI staining (B) or by FACS analysis (C). GFP$^+$ cells that contain the OKMS transgene and were SSEA1$^+$ (top right) were quantified as percentage of the total gated population. Scale bars represent 180 μm.

(D) BMP signaling enhances reprogramming of primary MEFs. Primary MEFs were transfected with OKMS *piggyBac* vectors and treated with Dox in the absence or presence of exogenous BMP7 (2 nM) for 9 days. The plates were then fixed and stained for SSEA1 and stained colonies counted. Data are the average SSEA1$^+$ colony number (±standard deviation) from three experiments. Subsequently, plates were stained with methylene-blue for macroscopic visualization of colonies as shown.

(E) iPSCs derived from BMP7-treated primary MEFs contribute to all three germ layers and adult mice. iPSCs generated in the presence of BMP7 added only during the initiation phase were aggregated with ICR (CD1 albino) morulae. Whole-mount LacZ staining of E10.5 chimeric embryos and cross-sectioning show extensive contribution of iPS LacZ-positive cells to derivatives of all three embryonic germ layers. Picture of chimeric mice obtained from a parallel litter are shown (bottom). Note the extensive contribution of BMP7-treated iPSCs (black coat color) to the pups. n, neural tube (ectoderm); m, mesenchyme (mesoderm); fg, foregut epithelium (endoderm) (top).

See also Figure S6.

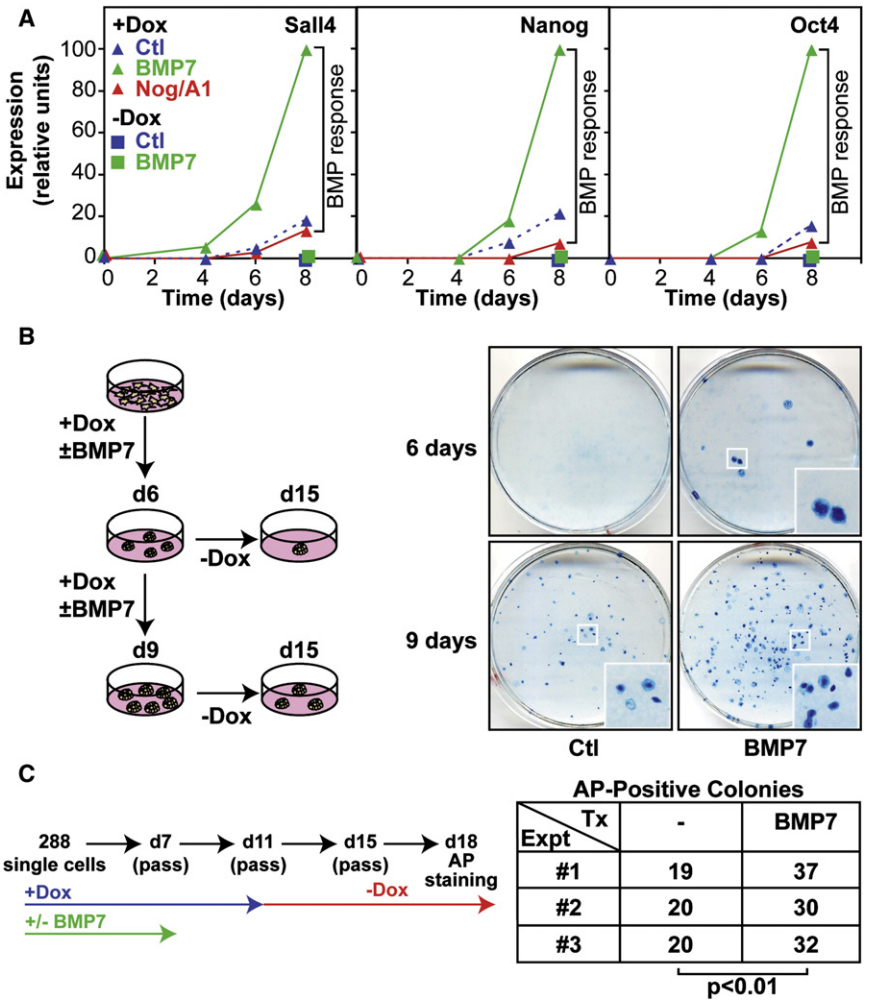

Figure 5. BMP Signaling Accelerates Reprogramming

(A) BMP signaling synergizes with OKMS to induce expression of ESC markers. 2°-6C MEFs were treated for 8 days without Dox in the presence or absence of BMP7 or for 4, 6, or 8 days with Dox in the presence or absence of BMP7 or Nog/A1, as indicated. mRNA levels for the ESC markers Nanog, Sall4, and Oct4 were then quantified by RT-qPCR and are plotted relative to the highest expression value of each gene.

(B) BMP signaling accelerates acquisition of independence from exogenous OKMS expression in reprogramming MEFs. Schematic of the protocol is presented on the left. 2°-6C MEFs were treated with Dox in the presence or absence of BMP7 (2 nM) for 6 days. At day 6, the cells were split into mESC media with Dox, in the presence or absence of BMP7 or into mESC media without Dox. At day 9, cells cultured in Dox were passaged into Dox-free mESC media. Dox-removed cells from day 6 and day 9 were cultured until day 15, then fixed and stained with methylene blue. Sample images of methylene-blue stained cells, treated with or without BMP7 for 6 or 9 days before Dox withdrawal, as indicated, are shown.

(C) BMP signaling enhances and accelerates reprogramming. In a single-cell assay, 288 2°-6C MEFs were seeded on feeders in 96-well plates and cultured according to the indicated schedule for 18 days. Plates were then stained for AP and scored for Dox-independent colonies. The number of AP-positive colonies obtained in three independent experiments (Exp) is shown. Tx, treatment.

either Mim-200c or Mim-200b reprogrammed much more efficiently (56% and 60% SSEA1$^+$ cells) and both mimics completely rescued the block in reprogramming caused by BMP antagonism. These studies show that induction of MET is the major function of BMP signaling during the initiation phase of reprogramming.

DISCUSSION

The ability to derive MEF populations that reprogram to a pluripotent state with relatively high efficiency by means of secondary MEFs indicates that reprogramming does not necessarily have to be a rare event and provides a powerful tool to explore the pathways of reprogramming. We exploited the Dox-regulated *piggyBac* reprogramming system (Woltjen et al., 2009) to conduct temporal expression profiling, which uncovered three phases of reprogramming: initiation, maturation, and stabilization (Figure 7F). A closer examination of the initiation phase identified an early, strong induction of mesenchymal-to-epithelial transition (MET) as one of the events taking place early in reprogramming. This MET is characterized by upregulation of epithelial junctional components, morphological transformation into epithelial-like colonies, and the appearance of Cdh1- and β-catenin-positive adherence junctions. Both AP and SSEA1 were concomitantly upregulated in these colonies, confirming that they had initiated reprogramming. Integration of our gene expression profiling data with the systematic functional RNAi screen results further demonstrated that both MET and BMP signaling are important for transiting initiation phase and led us to define a BMP-miRNA response that drives MET in MEFs. Our studies thus reveal synergistic interactions between OKMS and a BMP-miRNA-MET axis that accelerates progression through the initiation phase of reprogramming in MEFs.

Our temporal gene expression profiling of MEFs undergoing reprogramming showed phased patterns of expression. Although our work primarily focused on the initiation phase, the maturation phase was characterized by high expression of *Nanog* and *Sall4* (Chambers et al., 2003; Mitsui et al., 2003; Wu et al., 2006; Zhang et al., 2006). However, Nanog is also required in the context of reprogramming to attain a pluripotent state and its loss stalls reprogramming, whereas Sall4 enhances reprogramming but its expression is not absolutely required (Silva et al., 2009; Tsubooka et al., 2009). The induction of Nanog and Sall4 in maturation indicates that the gene expression

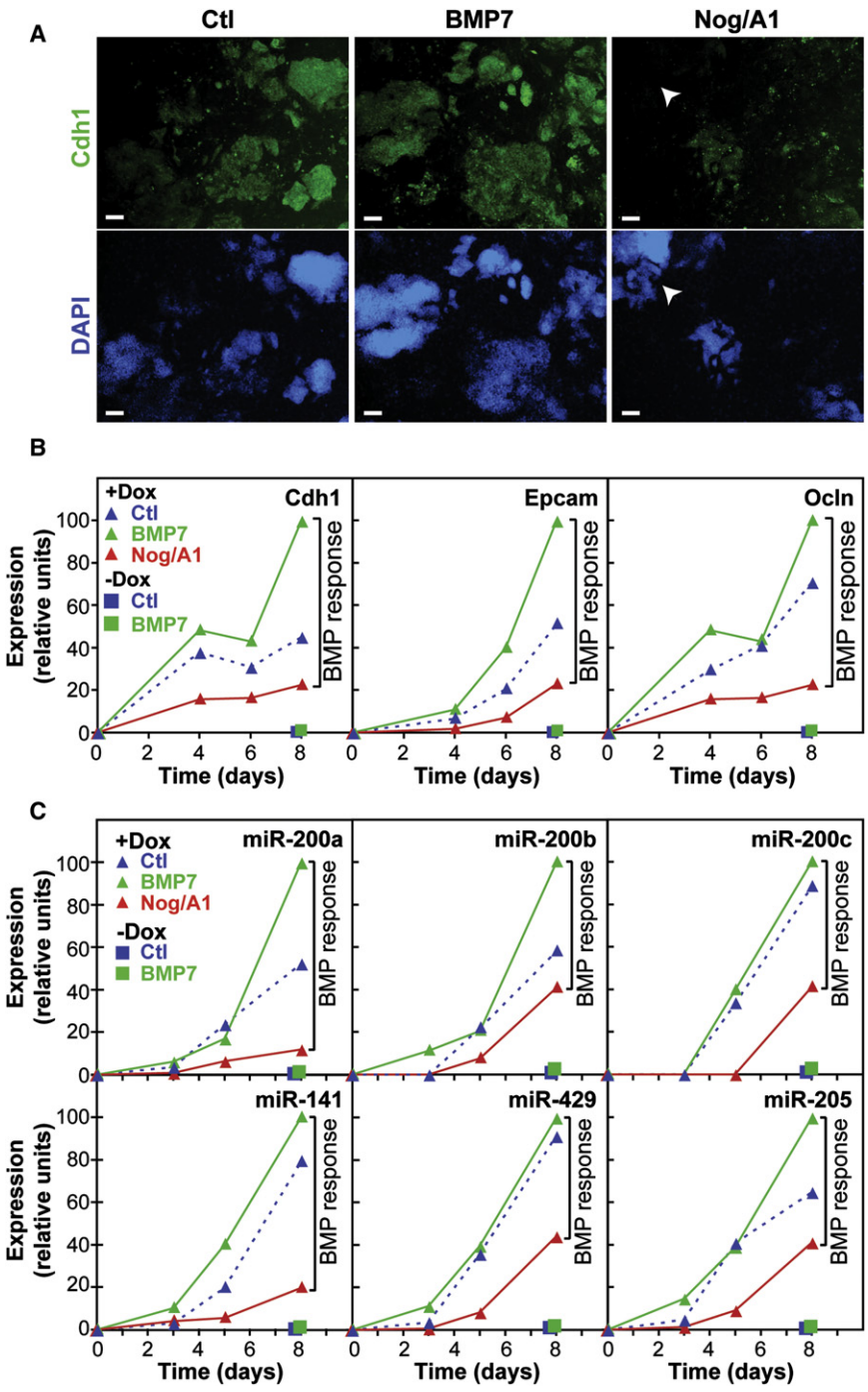

Figure 6. BMP Signaling Induces MET

(A) Cdh1 expression in reprogramming colonies is regulated by BMP signaling. 2°-6C MEFs were treated for 5 days with Dox in the absence or presence of either BMP7 or Nog/A1, as indicated. Cultures were then fixed and stained with Cdh1 and DAPI, and Cdh1-positive colonies visualized by immuno-fluorescence microscopy. White arrows point to a colony with undetectable Cdh1 expression. Scale bars represent 180 μm.

(B) BMP signaling synergizes with OKMS to induce expression of epithelial markers. 2°-6C MEFs were treated for 8 days without Dox in the presence or absence of BMP7 or for 4, 6, or 8 days with Dox in the presence or absence of BMP7 or Nog/A1, as indicated. mRNA levels for the epithelial markers Cdh1, Epcam, and Ocln were quantified by RT-qPCR and are plotted relative to the highest expression value of each gene.

(C) BMP signaling and OKMS synergistically induce expression of microRNAs regulating MET. 2°-6C MEFs were treated as indicated for 0, 3, 5, and 8 days. After total RNA extraction, the miRNA levels of miR-200 family members (miR-200a, -200b, -200c, -141, -429) and miR-205 were quantified by RT-qPCR. Results are plotted relative to the highest expression level for each microRNA.

changes associated with pluripotency begin relatively early in the reprogramming process. Accordingly, although a subset of pluripotency-associated genes is induced during maturation, other subsets were not induced until the later stabilization phase.

Our detailed analysis of the initiation phase revealed that BMP signaling synergizes with OKMS to induce miR-205 and miR-200 family members that in turn promote MET. Moreover, MET driven by miRNA-200 family mimics synergized with OKMS to accelerate reprogramming and removed the requirement for BMP signaling during this early phase. This suggests that the major function for BMP during the early phase of MEF reprogramming is to induce MET. However, MET is unlikely to be the only critical event during the initiation phase and we expect additional early events, such as epigenetic changes, to play critical roles in transiting reprogramming cells into the maturation phase. Collectively, these findings suggest that reprogramming the fibroblast genome is executed through a phased, hierarchical regulatory network (Figure 7F).

We also explored the stability of the initiation phase by inducing OKMS for 5 days followed by 5 days withdrawal. The majority of the gene expression changes resulting from OKMS induction returned to parental MEF levels after Dox withdrawal. Consistent with the rapid loss of reprogramming colonies, genes associated with the epithelial phenotype lost expression and the mesenchymal transcription factors of the Snail family returned to parental levels. These findings indicate that the initiation phase is both unstable and elastic, allowing reversion to the starting fate upon removal of OKMS. However, irreversible commitment to reprogramming probably occurs once Nanog and Sall4 are expressed, because these two factors are required and facilitate, respectively, the stable acquisition of pluripotency (Silva et al., 2009; Tsubooka et al., 2009). Consistent with this, we observed that removal of ectopic OKMS

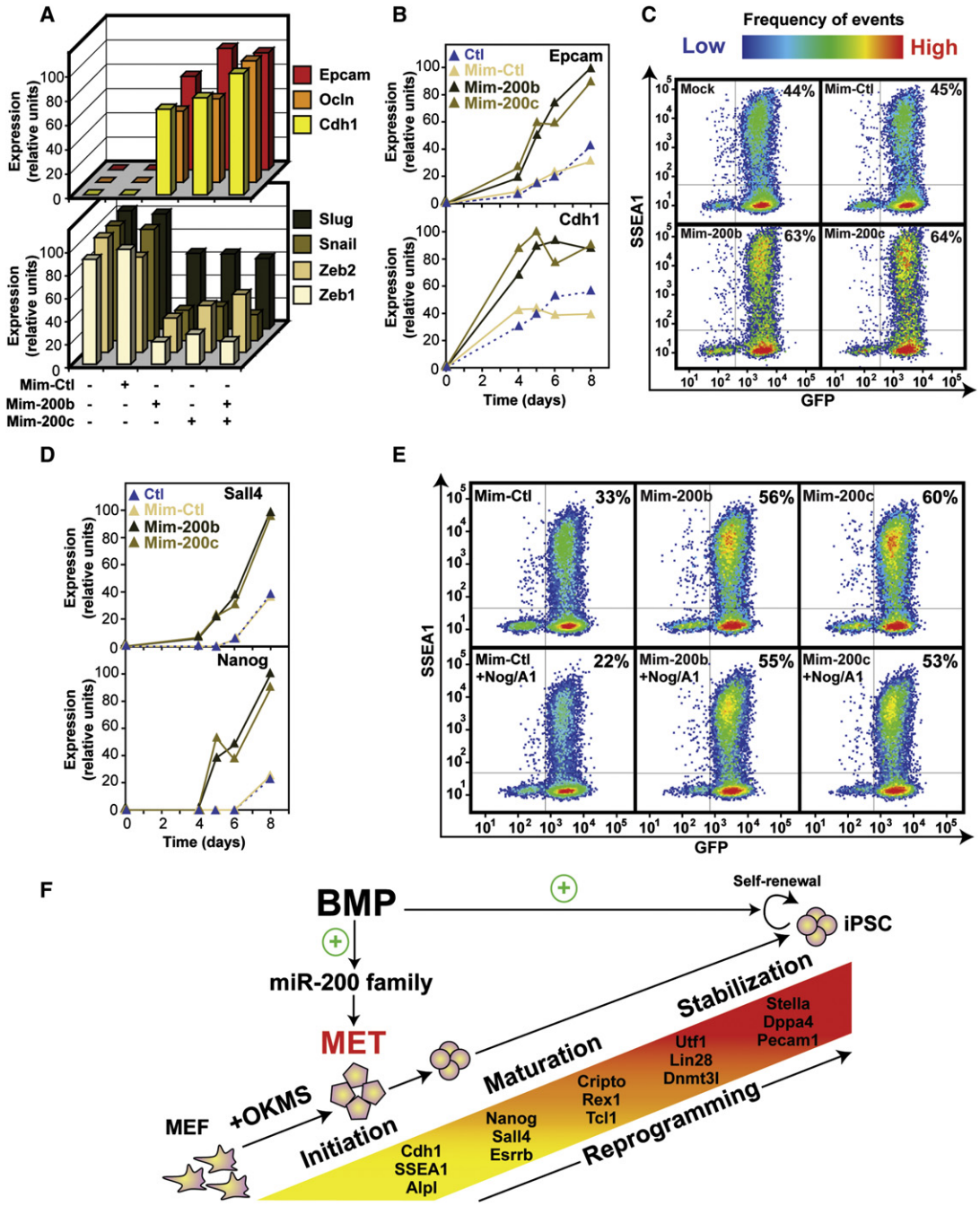

Figure 7. The miR-200 Family Members Synergize with OKMS to Promote Reprogramming

(A) Mimics (Mim) of miR-200b or miR-200c stimulate MET in MEFs. 2°-6C MEFs were transfected with 10 nM Mim-Ctl, Mim-200b, and Mim-200c either alone or in combination as indicated, and after 5 days in the absence of Dox, total RNA was extracted. mRNA levels of epithelial (top) or mesenchymal markers (bottom) were quantified by RT-qPCR. Results are plotted relative to the highest expression value for each gene.

(B) miR-200b and -200c mimics enhance Epcam and Cdh1 induction by OKMS. 2°-6C MEFs were transfected as in (A) in the presence of Dox for the indicated days. mRNA levels of epithelial markers, Cdh1 and Epcam, were analyzed by RT-qPCR and plotted relative to the highest expression value for each gene.

(C and D) The miR-200b and -200c synergize with OKMS to stimulate reprogramming. In (C), 2°-6C MEFs were transfected as described in (A) in the presence of Dox and analyzed by FACS after 5 days. GFP$^+$ cells that were also SSEA1$^+$ (top right) were quantified as percentage of the total gated population. In (D), 2°-6C MEFs were transfected as described in (A) in the presence of Dox. At the indicated time points, total RNA was extracted and Nanog and Sall4 mRNA levels were analyzed by RT-qPCR. Results are plotted relative to the highest expression value for each gene.

(E) The miR-200b and -200c mimics reverse the suppression of reprogramming by BMP antagonists. Cells were treated as in (C), in the presence or absence of the BMP antagonists Nog/A1, and analyzed by FACS after 5 days. GFP$^+$ cells that are SSEA1$^+$ (top right) were quantified as percentage of the total gated population.

expression at day 6, when *Nanog* and *Sall4* expression is just being initiated, led to rapid loss of colonies. In contrast, upon removal at day 9, when *Nanog* and *Sall4* are close to their peak expression levels, many Dox-independent colonies were observed. Accordingly, BMP treatment induced earlier and stronger induction of *Nanog* and *Sall4* and more rapid acquisition of a Dox-independent phenotype. We suggest that the onset of strong *Nanog* and *Sall4* expression marks the transition to the maturation phase, at which point elasticity is probably compromised.

To begin to unravel the mechanistic basis of reprogramming, we coupled expression profiling with a functional RNAi-based screen. This revealed a key role for intrinsic BMP signaling in synergizing with OKMS to induce MET during the initiation phase of MEF reprogramming. As of yet we do not know the molecular mechanism of BMP-OKMS synergism, but the context dependence of BMP-Smad responses is consistent with the dependence of Smads on physical interactions with DNA binding partners in order to efficiently target BMP-specific response elements (Attisano and Wrana, 2002). Furthermore, Smad1 co-occupies many of the regulatory regions bound by Oct4 and Sox2 in mESCs and Smad1 occupancy is dependent on Oct4 expression (Chen et al., 2008). This suggests that the synergism of BMP with OKMS during the initiation phase may be mediated via direct interactions of Smad1, Oct4, and Sox2 on transcriptional regulatory elements. Defining what components of OKMS mediate synergism with BMP-Smad signaling to induce MET and whether MET is a shared requirement for reprogramming of multiple cell types is thus an important area for future study.

BMP can induce differentiation in many contexts (Varga and Wrana, 2005), but also maintains pluripotency of mESCs in combination with LIF (Ying et al., 2003), with Nanog functioning to prevent BMP-induced differentiation (Suzuki et al., 2006). In the context of reprogramming, we showed a key role for BMP-driven MET during the initiation phase, prior to onset of *Nanog* expression. Thus, the strong induction of Nanog in the maturation phase may counteract differentiation signals and permit continued BMP signaling and the maintenance of the epithelial phenotype during later reprogramming steps. Although we have not functionally characterized BMP signaling to the end of reprogramming, we did find that epithelial-like junctions and morphology were retained in stably reprogrammed iPSCs. Furthermore, recent studies showed that FAB-SC that are maintained in FGF and Activin can be transitioned to a more primitive mESC state by continued growth in BMP and LIF that is dependent on Cdh1 (Chou et al., 2008). Moreover, constitutive expression of the miR-200 family members, miR-141, miR-200, and miR-429, which we show here promote MET and reprogramming even in the absence of BMP signaling, also can inhibit loss of pluripotency of mESCs in differentiating conditions (Lin et al., 2009). MET may be a fundamental cellular response that is required to reprogram a variety of cells lacking epithelial characteristics and maintain their pluripotent state. In this regard, it is interesting to note that recent studies have shown that TGF-β inhibitors promote reprogramming (Ichida et al., 2009; Maherali and Hochedlinger, 2009). Because TGF-β is a potent inducer of epithelial-to-mesenchymal transition (EMT) in some cells, it is tempting to speculate that inhibition of TGF-β may promote reprogramming by promoting MET. It will be interesting to define how factors that regulate the epithelial phenotype synergize with OKMS to promote progression through reprogramming.

Our comparative analysis of gene expression changes induced by OKMS in the early phase of reprogramming of two different 2° MEF lines showed similar sets of induced genes, in particular those associated with MET. However, OKMS also reprograms cell types of diverse origins, as do different cocktails of factors and chemical compounds. Comparative functional genomics analyses, as reported here, of reprogramming in distinct cell types or by distinct combinations of factors would thus be a powerful tool to distinguish whether all methods converge on a common path, or whether distinct paths can lead to a pluripotent state. Given the large number of gene expression changes noted during reprogramming, this would also facilitate dissecting passenger gene expression changes from those that drive reprogramming. Defining the functional pathways that underpin reprogramming will provide powerful tools to apply in a clinical context.

EXPERIMENTAL PROCEDURES

Reagents, Cell Culture, Teratoma Assays, and Cell Staining

Primary MEFs, 2°-6C, and 2°-1B cells were maintained in DMEM with high glucose, L-glutamine, and 10% FBS. All MEFs used for these experiments were less than passage 5. Cells were plated in MEF culture conditions and OKMS induced with 1.5 μg/mL Dox in standard mESC medium, as detailed in Supplemental Information. BMP7, Noggin, and A1/ECD were used at concentrations of 2 nM, 2 nM, and 1 nM, respectively. For teratoma assays, 1×10^6 iPSCs were injected in nude mice and teratomas extracted 6 weeks later as detailed in Supplemental Information. Chimeras were produced through aggregation of iPSC clumps with diploid Hsd:ICR(CD-1) embryos. LacZ-stained embryos were Dox induced in utero via ingestion for 24 hr prior to dissection. For microscopy, cells were cultured on gelatin-coated plates or chambered slides and fixed in 4% PFA at the indicated times. Details of protocols are described in Supplemental Information. All imaging and image analysis was performed with Volocity software (Improvision).

Microarray Analysis

For microarray analysis, RNA was isolated from 2°-6C and 2°-1B cells at the indicated time points and analyzed on Affymetrix mouse Exon Array 1.0 (TCAG Microarray Facility, HSC). RMA normalization was performed with Expression Console from Affymetrix and background subtraction implemented with the intron sequence negative controls. Time course expression data for 2°-6C MEF reprogramming was smoothed with Matlab and fold-changes calculated with Excel. Cluster 3.0 and Java TreeView were used for data centering, hierarchical clustering, and data visualization, respectively. Microarray expression data (Table S2) as well as detailed protocols are available in Supplemental Information.

Transfection of MEFs and siRNA Screening

For RNAi-mediated knockdown, siRNA (Dharmacon) were used at 40 nM and miRNA mimics (Dharmacon) at 10 nM. For siRNA transfection, MEFs were transfected with RNAiMAX (Invitrogen); for plasmids, MEFs were transfected with Fugene (Roche). For the RNAi screen, siRNA (Dharmacon) targeting

(F) The road to reprogramming. Model of MEF cells reprogramming kinetics, highlighting synergism between OKMS and the BMP-miRNA driven MET axis during the initiation phase.
See also Figure S7.

4010 distinct genes (Table S3) were cherry-picked at the SLRI SMART robotics facility. 2°-6C MEFs were coplated in mESC media containing Dox with siRNA mixed with RNAiMAX in OPTI-MEM for 16 hr. Cells were then washed into mESC containing 1.5 μg/mL Dox and cultured a further 5 days before fixing and staining for AP and DAPI as detailed in the Supplemental Information. Mock, siCtl, siNanog (negative controls), and siOct4 (positive control) were included on every plate. Once stained, five fields of individual wells were imaged with an InCell 1000 automated HCS microscope with a 4× objective and images quantitated with a custom algorithm developed in ImageJ, as detailed in the Supplemental Information. All transfections and staining were performed in the SLRI SMART robotics facility (http://robotics.lunenfeld.ca/).

FACS, Immunoblotting, and RT-qPCR

Immunoblotting and staining for FACS were performed with commercially available antibodies as detailed in Supplemental Information. For FACS analysis, cells were stained for SSEA1, then GFP and SSEA1 levels acquired on a BD FACS Canto flow cytometer (Becton Dickinson). $SSEA^+$ cell sorting was achieved with a BD FACS Aria. For RT-qPCR analysis, total RNA was extracted and absolute RT-qPCR was performed. Primers and detailed protocols are available in Supplemental Information.

Statistical Analysis and Replicates

All data presented are representative of at least three independent experiments that yielded similar results. Statistical analyses were performed with the software Prism (Graphpad) and Matlab 7.7 (MathWorks).

ACCESSION NUMBERS

Microarray data were deposited in NCBI GEO database with accession number GSE21757.

SUPPLEMENTAL INFORMATION

Supplemental Information includes Supplemental Experimental Procedures, five figures, and three tables and can be found with this article online at doi:10.1016/j.stem.2010.04.015.

ACKNOWLEDGMENTS

The authors thank T. Sun and F. Vizeacoumar for assistance with robotics, J. Audet for the FACS machine, M. Gertsenstein and M. Pereira for the chimera production, M. Narimatsu for helping with chimera processing, M. Mileikovkaia for advice, J. Ellis for discussions, and L. Attisano for critical review of the manuscript. This work was supported by funds from CIHR (to J.L.W. grant #MOP12860 and A.N. grant #MOP-210751), the Canadian Stem Cell Network (J.L.W. and A.N.), and the Ontario Ministry of Resource and Innovation (J.L.W.). L.D. and P.S.-T. are CIHR Fellowship recipients and T.A.B. is a Swish National Science Foundation Fellowship recipient. A.N. is a CRC Chair in Stem Cell and Regeneration. J.L.W. is an HHMI International Scholar and CRC Chair in Systems Biology.

Received: October 9, 2009
Revised: March 9, 2010
Accepted: April 26, 2010
Published online: June 17, 2010

REFERENCES

Attisano, L., and Wrana, J.L. (2002). Signal transduction by the TGF-beta superfamily. Science *296*, 1646–1647.

Bracken, C.P., Gregory, P.A., Kolesnikoff, N., Bert, A.G., Wang, J., Shannon, M.F., and Goodall, G.J. (2008). A double-negative feedback loop between ZEB1-SIP1 and the microRNA-200 family regulates epithelial-mesenchymal transition. Cancer Res. *68*, 7846–7854.

Brambrink, T., Foreman, R., Welstead, G.G., Lengner, C.J., Wernig, M., Suh, H., and Jaenisch, R. (2008). Sequential expression of pluripotency markers during direct reprogramming of mouse somatic cells. Cell Stem Cell *2*, 151–159.

Chambers, I., Colby, D., Robertson, M., Nichols, J., Lee, S., Tweedie, S., and Smith, A. (2003). Functional expression cloning of Nanog, a pluripotency sustaining factor in embryonic stem cells. Cell *113*, 643–655.

Chen, X., Xu, H., Yuan, P., Fang, F., Huss, M., Vega, V.B., Wong, E., Orlov, Y.L., Zhang, W., Jiang, J., et al. (2008). Integration of external signaling pathways with the core transcriptional network in embryonic stem cells. Cell *133*, 1106–1117.

Chou, Y.F., Chen, H.H., Eijpe, M., Yabuuchi, A., Chenoweth, J.G., Tesar, P., Lu, J., McKay, R.D., and Geijsen, N. (2008). The growth factor environment defines distinct pluripotent ground states in novel blastocyst-derived stem cells. Cell *135*, 449–461.

David, L., Mallet, C., Keramidas, M., Lamandé, N., Gasc, J.M., Dupuis-Girod, S., Plauchu, H., Feige, J.J., and Bailly, S. (2008). Bone morphogenetic protein-9 is a circulating vascular quiescence factor. Circ. Res. *102*, 914–922.

Furusawa, T., Ikeda, M., Inoue, F., Ohkoshi, K., Hamano, T., and Tokunaga, T. (2006). Gene expression profiling of mouse embryonic stem cell subpopulations. Biol. Reprod. *75*, 555–561.

Gregory, P.A., Bert, A.G., Paterson, E.L., Barry, S.C., Tsykin, A., Farshid, G., Vadas, M.A., Khew-Goodall, Y., and Goodall, G.J. (2008). The miR-200 family and miR-205 regulate epithelial to mesenchymal transition by targeting ZEB1 and SIP1. Nat. Cell Biol. *10*, 593–601.

Gurdon, J.B. (1964). The transplantation of living cell nuclei. Adv. Morphog. *4*, 1–43.

Herrera, B., and Inman, G.J. (2009). A rapid and sensitive bioassay for the simultaneous measurement of multiple bone morphogenetic proteins. Identification and quantification of BMP4, BMP6 and BMP9 in bovine and human serum. BMC Cell Biol. *10*, 20.

Ichida, J.K., Blanchard, J., Lam, K., Son, E.Y., Chung, J.E., Egli, D., Loh, K.M., Carter, A.C., Di Giorgio, F.P., Koszka, K., et al. (2009). A small-molecule inhibitor of tgf-Beta signaling replaces sox2 in reprogramming by inducing nanog. Cell Stem Cell *5*, 491–503.

Korpal, M., Lee, E.S., Hu, G., and Kang, Y. (2008). The miR-200 family inhibits epithelial-mesenchymal transition and cancer cell migration by direct targeting of E-cadherin transcriptional repressors ZEB1 and ZEB2. J. Biol. Chem. *283*, 14910–14914.

Lin, C.H., Jackson, A.L., Guo, J., Linsley, P.S., and Eisenman, R.N. (2009). Myc-regulated microRNAs attenuate embryonic stem cell differentiation. EMBO J. *28*, 3157–3170.

Maherali, N., and Hochedlinger, K. (2009). Tgfbeta signal inhibition cooperates in the induction of iPSCs and replaces Sox2 and cMyc. Curr. Biol. *19*, 1718–1723.

Maherali, N., Sridharan, R., Xie, W., Utikal, J., Eminli, S., Arnold, K., Stadtfeld, M., Yachechko, R., Tchieu, J., Jaenisch, R., et al. (2007). Directly reprogrammed fibroblasts show global epigenetic remodeling and widespread tissue contribution. Cell Stem Cell *1*, 55–70.

Maherali, N., Ahfeldt, T., Rigamonti, A., Utikal, J., Cowan, C., and Hochedlinger, K. (2008). A high-efficiency system for the generation and study of human induced pluripotent stem cells. Cell Stem Cell *3*, 340–345.

Mikkelsen, T.S., Hanna, J., Zhang, X., Ku, M., Wernig, M., Schorderet, P., Bernstein, B.E., Jaenisch, R., Lander, E.S., and Meissner, A. (2008). Dissecting direct reprogramming through integrative genomic analysis. Nature *454*, 49–55.

Mitsui, K., Tokuzawa, Y., Itoh, H., Segawa, K., Murakami, M., Takahashi, K., Maruyama, M., Maeda, M., and Yamanaka, S. (2003). The homeoprotein Nanog is required for maintenance of pluripotency in mouse epiblast and ES cells. Cell *113*, 631–642.

Müller, F.J., Laurent, L.C., Kostka, D., Ulitsky, I., Williams, R., Lu, C., Park, I.H., Rao, M.S., Shamir, R., Schwartz, P.H., et al. (2008). Regulatory networks define phenotypic classes of human stem cell lines. Nature *455*, 401–405.

Okita, K., Ichisaka, T., and Yamanaka, S. (2007). Generation of germline-competent induced pluripotent stem cells. Nature *448*, 313–317.

Silva, J., Nichols, J., Theunissen, T.W., Guo, G., van Oosten, A.L., Barrandon, O., Wray, J., Yamanaka, S., Chambers, I., and Smith, A. (2009). Nanog is the gateway to the pluripotent ground state. Cell *138*, 722–737.

Sridharan, R., Tchieu, J., Mason, M.J., Yachechko, R., Kuoy, E., Horvath, S., Zhou, Q., and Plath, K. (2009). Role of the murine reprogramming factors in the induction of pluripotency. Cell *136*, 364–377.

Suzuki, A., Raya, A., Kawakami, Y., Morita, M., Matsui, T., Nakashima, K., Gage, F.H., Rodríguez-Esteban, C., and Izpisúa Belmonte, J.C. (2006). Nanog binds to Smad1 and blocks bone morphogenetic protein-induced differentiation of embryonic stem cells. Proc. Natl. Acad. Sci. USA *103*, 10294–10299.

Takahashi, K., and Yamanaka, S. (2006). Induction of pluripotent stem cells from mouse embryonic and adult fibroblast cultures by defined factors. Cell *126*, 663–676.

Thiery, J.P., Acloque, H., Huang, R.Y., and Nieto, M.A. (2009). Epithelial-mesenchymal transitions in development and disease. Cell *139*, 871–890.

Tsubooka, N., Ichisaka, T., Okita, K., Takahashi, K., Nakagawa, M., and Yamanaka, S. (2009). Roles of Sall4 in the generation of pluripotent stem cells from blastocysts and fibroblasts. Genes Cells *14*, 683–694.

Vallier, L., Mendjan, S., Brown, S., Chng, Z., Teo, A., Smithers, L.E., Trotter, M.W., Cho, C.H., Martinez, A., Rugg-Gunn, P., et al. (2009). Activin/Nodal signalling maintains pluripotency by controlling Nanog expression. Development *136*, 1339–1349.

Varga, A.C., and Wrana, J.L. (2005). The disparate role of BMP in stem cell biology. Oncogene *24*, 5713–5721.

Wernig, M., Meissner, A., Foreman, R., Brambrink, T., Ku, M., Hochedlinger, K., Bernstein, B.E., and Jaenisch, R. (2007). In vitro reprogramming of fibroblasts into a pluripotent ES-cell-like state. Nature *448*, 318–324.

Wernig, M., Lengner, C.J., Hanna, J., Lodato, M.A., Steine, E., Foreman, R., Staerk, J., Markoulaki, S., and Jaenisch, R. (2008). A drug-inducible transgenic system for direct reprogramming of multiple somatic cell types. Nat. Biotechnol. *26*, 916–924.

Woltjen, K., Michael, I.P., Mohseni, P., Desai, R., Mileikovsky, M., Hämäläinen, R., Cowling, R., Wang, W., Liu, P., Gertsenstein, M., et al. (2009). piggyBac transposition reprograms fibroblasts to induced pluripotent stem cells. Nature *458*, 766–770.

Wu, Q., Chen, X., Zhang, J., Loh, Y.H., Low, T.Y., Zhang, W., Zhang, W., Sze, S.K., Lim, B., and Ng, H.H. (2006). Sall4 interacts with Nanog and co-occupies Nanog genomic sites in embryonic stem cells. J. Biol. Chem. *281*, 24090–24094.

Xu, D., Alipio, Z., Fink, L.M., Adcock, D.M., Yang, J., Ward, D.C., and Ma, Y. (2009). Phenotypic correction of murine hemophilia A using an iPS cell-based therapy. Proc. Natl. Acad. Sci. USA *106*, 808–813.

Ying, Q.L., Nichols, J., Chambers, I., and Smith, A. (2003). BMP induction of Id proteins suppresses differentiation and sustains embryonic stem cell self-renewal in collaboration with STAT3. Cell *115*, 281–292.

Zhang, J., Tam, W.L., Tong, G.Q., Wu, Q., Chan, H.Y., Soh, B.S., Lou, Y., Yang, J., Ma, Y., Chai, L., et al. (2006). Sall4 modulates embryonic stem cell pluripotency and early embryonic development by the transcriptional regulation of Pou5f1. Nat. Cell Biol. *8*, 1114–1123.

Zhao, R., and Daley, G.Q. (2008). From fibroblasts to iPS cells: Induced pluripotency by defined factors. J. Cell. Biochem. *105*, 949–955.

Zhao, T., and Xu, Y. (2010). p53 and stem cells: New developments and new concerns. Trends Cell Biol. *20*, 170–175.